Pseudo-Goldstone excitations in a striped Bose-Einstein condensate

Guan-Qiang Li,[1,2] Xi-Wang Luo,[1,*] Junpeng Hou,[1] and Chuanwei Zhang[1,†]
[1]*Department of Physics, The University of Texas at Dallas, Richardson, Texas 75080-3021, USA*
[2]*School of Arts and Sciences, Shaanxi University of Science and Technology, 710021 Xi'an, China*

(Received 19 January 2021; accepted 19 July 2021; published 12 August 2021)

Significant experimental progress has been made recently for observing long-sought supersolidlike states in Bose-Einstein condensates, where spatial translational symmetry is spontaneously broken by anisotropic interactions to form a stripe order. Meanwhile, the superfluid stripe ground state was also observed by applying a weak optical lattice that forces the symmetry breaking. Despite the similarity of the ground states, here we show that these two symmetry breaking mechanisms can be distinguished by their collective excitation spectra. In contrast to gapless Goldstone modes of the *spontaneous* stripe state, we propose that the excitation spectra of the *forced* stripe phase can provide direct experimental evidence for the gapped pseudo-Goldstone modes. We characterize the pseudo-Goldstone mode of such lattice-induced stripe phase through its excitation spectrum and static structure factor. Our work may pave the way for exploring spontaneous and forced or approximate symmetry breaking mechanisms in different physical systems.

DOI: 10.1103/PhysRevA.104.023311

I. INTRODUCTION

Spontaneous symmetry breaking plays a crucial role for the understanding of many important phenomena in different fields ranging from elementary particles to condensed states of matter. For instance, crystalline and superfluidity orders are formed in the long-sought supersolids through spontaneously breaking spatial translational and $U(1)$ gauge symmetries [1]. While the early study of supersolidity focused on solid ^{4}He [2,3] without conclusive experimental evidence [4,5], ultracold atoms have emerged as a powerful platform in recent years for observing supersolidlike quantum phases [6–14]. Significant experimental progress has been made on the generation and measurement of supersolidlike superfluid stripe states in both dipolar [10–13] and spin-orbit-coupled Bose-Einstein condensates (BECs) [14], where spontaneous translational symmetry breaking is driven by dipolar or anisotropic spin interactions. In the latter case, the anisotropic spin interactions favor the occupation of both band minima of the spin-orbit coupling induced double-well dispersion, yielding superfluid stripe phase with periodic density modulations [15–23].

In the region where ground state symmetry cannot be spontaneously broken by interactions, the symmetry breaking ground state may be achieved by applying a weak symmetry breaking potential. Such a forced symmetry breaking mechanism has been demonstrated recently in a spin-orbit-coupled BEC, where the superfluid stripe ground state is realized by applying a weak optical lattice [24] that breaks translational symmetry explicitly. Interestingly, the forced stripe ground state shows similar (spin-)density patterns as the spontaneous one induced solely by the anisotropic atomic interactions. Therefore two questions naturally arise: Can we distinguish the stripe ground states resulting from spontaneous and forced symmetry breaking mechanisms? If so, are there interesting experimental observables? These questions should also apply to general spontaneous and forced symmetry breaking ground states in other physical systems.

In this paper, we address these two important questions by investigating the collective excitations of the forced superfluid stripe ground state and show that the emerging pseudo-Goldstone spectrum lies at the heart of understanding its forced symmetry breaking. The pseudo-Goldstone mode is an important concept in fields ranging from standard model to solid-state materials [25–27], with prominent examples including the pion (the lightest hardon) [28,29] and longitudinal polarization components of W and Z bosons in high-energy physics [30], phonon modes in superconductors and/or superfluids [31–34], and magnons in magnets [35–37]. However, direct experimental observation of the pseudo-Goldstone spectrum remains challenging. The capability of directly measuring the excitation spectrum using Bragg spectroscopy [38–43] in ultracold atomic gases thus provides a powerful tool for probing the pseudo-Goldstone spectrum. Our main results are as follows:

(i) In the strong anisotropic spin interaction region, the spontaneous superfluid stripe ground state hosts two gapless Goldstone modes. A weak lattice breaks the translational symmetry (i.e., the symmetry is approximate) and turns one gapless mode into a pseudo-Goldstone mode, which is characterized by the gap of the excitation spectrum at the long wavelength limit (i.e., zero-momentum gap). The hybridization of the gapped pseudo-Goldstone and the remaining gapless modes yields an avoided-crossing gap at a finite momentum.

(ii) In the weak anisotropic spin interaction region, an increasing lattice potential forces a transition from plane-wave to stripe ground states. The zero momentum

*Corresponding author: xiwang.luo@utdallas.edu
†Corresponding author: chuanwei.zhang@utdallas.edu

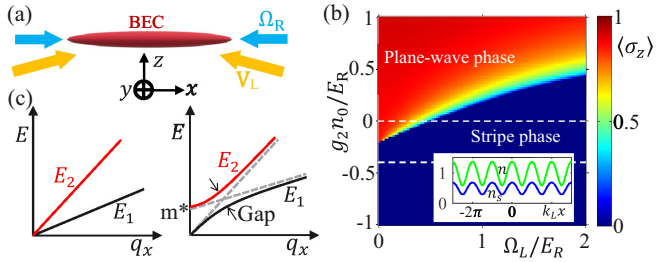

FIG. 1. (a) Scheme to generate spin-orbit coupling and optical lattice for a trapped BEC. (b) Phase diagram in the g_2-Ω_L plane, with $\Omega_R = 2.0E_R$, $\delta = 0$, $gn_0 = 1.0E_R$ and n_0 the mean atom density. Two bold dashed lines correspond to the weak and strong spin interactions regimes for Figs. 2–4. The inset shows the typical densities (normalized to n_0) of spin-up (or spin-down) component (blue line) and the total density (green line). (c) Schematic illustration of the two (pseudo-)Goldstone modes without (left panel) and with (right panel) a weak and explicitly symmetry-breaking term.

pseudo-Goldstone gap first decreases to zero at the phase transition point and then reopens. In the forced superfluid stripe region, the properties of gapped excitation spectrum (e.g., zero-momentum and avoided-crossing gaps) largely resemble those for spontaneous superfluid stripe phase subject to a weak lattice perturbation (i.e., approximate symmetry), demonstrating that it is a pseudo-Goldstone spectrum. The forced superfluid stripe ground state is experimentally more accessible and robust than the spontaneous one, opening the pathway for the direct observation of pseudo-Goldstone spectrum in experiments.

(iii) The structure factors of the two lowest energy modes show that gapless Goldstone and gapped pseudo-Goldstone branches correspond to density (phonon) and spin-density (magnon) modes, respectively. The static structure factor for the spin density reveals some differences between spontaneous and forced superfluid stripe ground states due to their different stripe formation mechanisms. The excitation spectrum and structure factor can be detected in experiments through Bragg scattering.

II. MODEL

We consider the experimental setup illustrated in Fig. 1(a). The BEC is confined in a cigar-shaped optical dipole trap, with spin-orbit coupling along the x direction realized by two Raman laser beams, which couple the two pseudospin states $|\uparrow\rangle$ and $|\downarrow\rangle$ (e.g., $|1,-1\rangle$ and $|1,0\rangle$ of ^{87}Rb atoms within the $F = 1$ hyperfine manifold) with momentum kick $2k_R$ (k_R is the recoil momentum). In addition, we consider a weak optical lattice $V_L(x) = 2\Omega_L \sin^2(k_L x)$. The single-particle Hamiltonian in the spin basis (with momentum and energy units as $\hbar k_R$ and $\frac{\hbar^2 k_R^2}{2m}$) reads

$$H_0 = (i\partial_x + \sigma_z)^2 - \frac{\delta}{2}\sigma_z + \frac{\Omega_R}{2}\sigma_x + V_L(x), \tag{1}$$

where Ω_R is the strength of the Raman coupling and δ is the detuning of the two-photon Raman transition. Spin-orbit coupling induces a momentum-space double-well band dispersion, and the period of the optical lattice is set such that $2k_L$ equals the separation between two band minima.

We first find the ground state $\psi_{0s}(x)$ by imaginary-time evolution of the Gross-Pitaevskii (GP) equation

$$i\frac{\partial\psi_s(x,t)}{\partial t} = H_{\rm GP}(\psi_s)\psi_s(x,t), \tag{2}$$

where ψ_s is the spinor wave function with $s = \uparrow, \downarrow$ and $H_{\rm GP}(\psi_s) = H_0 + gn + g_2|\psi_{\bar{s}}|^2$ with n the total density (see Appendix A). We have assumed the intraspin interaction as $g_{\uparrow\uparrow} = g_{\downarrow\downarrow} = g$ and the anisotropic spin interaction as $g_2 = g_{\uparrow\downarrow} - g$, with $g_{ss'}$ the interaction strength between atoms in s and s' states. The phase diagram in the g_2-Ω_L plane is shown in Fig. 1(b) [typical (spin-)density distributions of the stripe state are shown in the inset]. The system favors the stripe phase (plane-wave phase) for large negative (positive) g_2 (note that the stripe and plane-wave phases become the unpolarized and polarized Bloch states in the presence of a lattice). The phase boundary lies at the weak anisotropic interaction region around $g_2 = 0$, and the critical value of g_2 increases with the lattice strength (see Appendix B for more details).

Without the optical lattice, the stripe phase occupying both band minima can be formed in the system under the antiferromagnetic atomic interaction ($g_2 < 0$) [15–18]. Typically, the stripe phase only exits for very weak Ω_R and δ due to the weak anisotropy of interaction $|g_2|$ in realistic experiments, making its observation difficult. This may be overcome by using atoms with strong anisotropic spin interactions, or alternatively, by adding a weak optical lattice that couples the two band minima directly. The latter approach has led to the recent observation of a long-lived superstripe state using ^{87}Rb atoms [24]. We want to point out that there is a tiny difference between the ground-state stripe period at $\Omega_L = 0$ and the optical lattice period. The two periods would match as long as the optical lattice strength is not extremely small.

The forced stripe ground state induced by symmetry-breaking potential shows similar (spin-)density patterns as the spontaneous one induced solely by the anisotropic interactions. To characterize and distinguish the stripe states formed under different symmetry breaking mechanisms, we consider the excitation spectrum. For spontaneous stripe phase induced solely by interactions, both the $U(1)$ gauge and continuous translational symmetries are broken spontaneously, leading to two gapless Goldstone modes [as illustrated in the left panel of Fig. 1(c)] [44–46]. When the translational symmetry is weakly broken by a lattice perturbation (i.e., the symmetry is now approximate), we expect to observe the gap opening of one Goldstone mode (equivalent to an effective mass m^* of the corresponding Goldstone boson). If the lower mode becomes a gapped pseudo-Goldstone mode, there should be an avoided crossing due to the hybridization of the two original Goldstone modes [as illustrated in the right panel of Fig. 1(c)].

To obtain the spectrum of elementary excitations, we write the deviations of the wave functions with respect to the ground state as

$$\psi_s(x,t) = e^{-i\mu t}\left[\psi_{0s}(x) + u_s(x)e^{-i\varepsilon t} + v_s^*(x)e^{i\varepsilon t}\right]. \tag{3}$$

The amplitudes $u_s(x)$ and $v_s(x)$ satisfy normalization condition $\sum_s \int_0^d dx[|u_s(x)|^2 - |v_s(x)|^2] = 1$, with d the stripe period and μ the chemical potential. Substituting Eq. (3) into Eq. (2), we obtain the Bogoliubov equation as $\varepsilon[u_\uparrow, u_\downarrow, v_\uparrow, v_\downarrow]^T = \mathcal{H}[u_\uparrow, u_\downarrow, v_\uparrow, v_\downarrow]^T$. The expression of

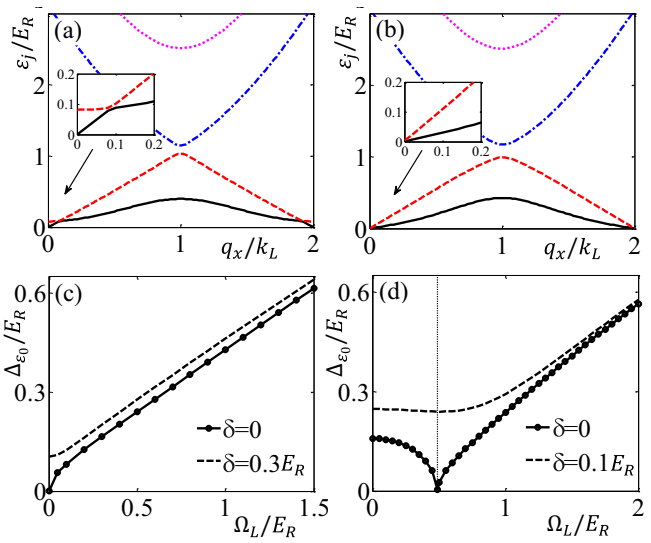

FIG. 2. (a),(b) Low-energy spectra of the elementary excitations for the stripe phase. (c),(d) Change of the zero-momentum gap Δ_{ε_0} with the lattice strength Ω_L. Panels (a),(c) and (b),(d) are for strong ($g_2 n_0 = -0.4E_R$) and weak ($g_2 n_0 = -0.005E_R$) anisotropic spin interactions, respectively. The lattice strength $\Omega_L = 0.1E_R$ in (a), and $\Omega_L^c = 0.4871E_R$ in (b) is the phase transition point between the plane-wave phase and the stripe phase. The dashed lines in (c) and (d) represent nonzero detunings. The dotted line in (d) corresponds to Ω_L^c. $gn_0 = 1.0E_R$ and $\Omega_R = 2.0E_R$.

the Bogoliubov Hamiltonian $\mathcal{H}$ is given in Appendix C, and the excitation spectra can be calculated numerically by expanding $u_s(x)$ and $v_s(x)$ in the Bloch basis. Each excitation spectrum is periodic in momentum space with the Brillouin zone determined by the stripe period.

III. PSEUDO-GOLDSTONE SPECTRUM

We focus mainly on the elementary excitations under the situation of the antiferromagnetic atomic interaction (i.e., $g_2 < 0$), where the stripe phase mainly resides. For a typical Raman coupling $\Omega_R \gtrsim E_R$, the system prefers to form the stripe (plane-wave) phase under strong (weak) anisotropic spin interaction $|g_2|$ in the absence of optical lattices. We first consider the strong anisotropic spin interaction with a weak optical lattice [lower region in Fig. 1(b)]. The optical lattice slightly breaks the space translational symmetry of the system yet alters the excitation spectrum dramatically. The low-energy bands in the first Brillouin zone with weak optical lattice are demonstrated in Fig. 2(a). The double gapless spectrum disappears and a gap Δ_{ε_0} in the second band at zero Bloch momentum ($q_x = 0$) is opened, which corresponds to the generation of the pseudo-Goldstone mode of the system at the long wavelength limit. The pseudo-Goldstone mode is generated once the lattice is turned on. The change of the zero-momentum gap Δ_{ε_0} with the strength of the optical lattice is given in Fig. 2(c). The gap vanishes at zero lattice strength and increases with increasing optical lattice strength. The size of the gap almost changes linearly with the optical lattice except near the zero momentum. A small detuning δ would hardly affect the spectrum, while a large δ may drive the system out of the stripe phase and lead to a roton gap ($\Delta_{\varepsilon_0} > 0$) at $\Omega_L = 0$. The effect of δ is diminished at larger lattice strength.

With decreasing anisotropic spin interaction $|g_2|$, the system is driven from the stripe phase into the plane-wave phase (i.e., the polarized Bloch state). The pseudo-Goldstone gap Δ_{ε_0} decreases to zero at the critical phase boundary and then reopens as a nonzero roton gap. Further increasing lattice strength can drive the transition from the polarized Bloch state to the stripe phase, where roton gap Δ_{ε_0} decreases to zero at the critical phase boundary and then reopens as the pseudo-Goldstone gap [see Fig. 2(d)]. Notice that at the phase boundary, the excitation spectrum of the forced stripe state is very similar to that for strong anisotropic interaction with two gapless Goldstone modes [see Fig. 2(b)]. For weak anisotropic spin interactions ($g_2 \simeq 0$), the phase transition boundary locates at the lattice strength $\Omega_L^c = 0.4871E_R$. Beyond the critical lattice strength Ω_L^c, the pseudo-Goldstone gap [see Fig. 2(d)] behaves similarly as that in the strong anisotropic interaction regime [see Fig. 2(c)], demonstrating the properties of the pseudo-Goldstone spectrum. Therefore, the forced superfluid stripe ground state, which is experimentally more accessible and robust than the spontaneous one, opens the pathway for the direct observation of the pseudo-Goldstone spectrum in experiments utilizing techniques that have already been used to study the spectrum of elementary excitations for spin-orbit-coupled BECs [40,41], quantum gas with cavity-mediated long-range interactions [42], and BEC in a shaken optical lattice [43].

The pseudo-Goldstone mode near the phase boundary results from the interplay between the interaction and optical lattice, which tends to reduce the spatial modulation of the GP Hamiltonian $H_{\rm GP}(\psi_{0s})$ for the ground state. In the vicinity of the phase boundary, $H_{\rm GP}(\psi_{0s})$ preserves an approximate translational symmetry (see Appendix B), which leads to a vanishing gap of the pseudo-Goldstone mode. On the other hand, the pseudo-Goldstone mode for strong $|g_2|$ with a very weak lattice is induced by the approximate translational symmetry of H_0, while $H_{\rm GP}(\psi_{0s})$ strongly breaks the translational symmetry. In the presence of nonzero detuning δ, the phase boundary becomes a crossover boundary, and Δ_{ε_0} decreases to a finite value as the system goes from the stripe region to the plane-wave region, where Δ_{ε_0} is almost a constant [see Fig. 2(d)]. The effects of the Raman coupling and the atomic interactions on Δ_{ε_0} are given in Appendix C.

IV. AVOIDED SPECTRUM CROSSING

In addition to the zero-momentum gap, there exists another avoided crossing gap $\Delta_{\rm ac}$ (the minimum value of the gap between the first and second bands), originating from the hybridization between the pseudo-Goldstone and Goldstone modes. The nonzero-momentum gap $\Delta_{\rm ac}$ as a function of the lattice strength for strong anisotropic spin interaction is given in Fig. 3(a). The gap increases slowly with increasing lattice strength at the beginning, and then rapidly in the deep lattice region. In contrast, the avoided crossing point $q_{\rm ac}$ first increases rapidly with the lattice strength, and remains saturated in the deep lattice region. Figure 3(b) shows $\Delta_{\rm ac}$ as a function of lattice strength for weak anisotropic spin interaction. In the plane-wave phase, $\Delta_{\rm ac}$ first increases with

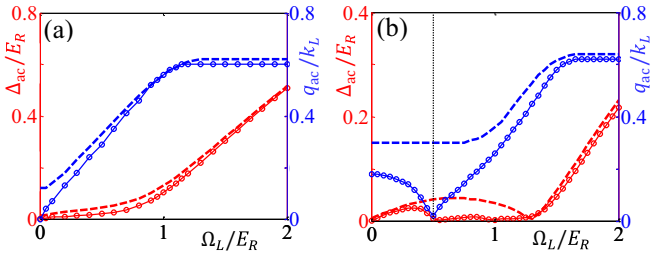

FIG. 3. Change of the size Δ_{ac} and position q_{ac} of the nonzero-momentum gap with the lattice strength Ω_L. The parameters in (a) and (b) are the same as those in Figs. 2(c) and 2(d). The dashed lines represent nonzero detuning $|\delta| = 0.3E_R$ in (a) and $|\delta| = 0.1E_R$ in (b), respectively. The gray dotted line in (b) corresponds to the phase transition point $\Omega_L^c = 0.4871E_R$.

the lattice strength and then decreases to zero at the phase boundary, while q_{ac} decreases directly to zero. In the stripe phase, Δ_{ac} and q_{ac} behave similarly as those for the strong anisotropic spin interaction [see Fig. 3(a)]. A nonzero Raman detuning δ tends to increase both the gap Δ_{ac} and its position q_{ac} [see the dashed lines in Fig. 3(a) and 3(b)]. The effect of the Raman coupling on Δ_{ac} and q_{ac} are given in Appendix C.

V. STRUCTURE FACTORS

As discussed above, the pseudo-Goldstone spectra for the weak and strong anisotropic spin interactions are very similar, although the ground stripe phases are achieved through different symmetry breaking mechanisms. In experiments, the collective properties of the excitation spectrum of the BECs can be probed using Bragg spectroscopy, which measures the dynamical structure factors. For a scattering probe with momentum $\hbar q_x$ and energy $\hbar\omega$, the dynamical structure factor takes the form [44,47]

$$S(q_x, \omega) = \sum_j |\langle j|\rho^\dagger_{q_x}|0\rangle|^2 \tilde{\delta}(\hbar\omega - \varepsilon_j) \tag{4}$$

with $|j\rangle$ the excited state, ε_j the excitation energy, $\rho_{q_x} = \sum_j e^{iq_x x_j/\hbar}$ the density operator, and $\tilde{\delta}(\cdot)$ the Dirac delta function. The excitation strength $Z_j = |\langle j|\rho^\dagger_{q_x}|0\rangle|^2$ can be evaluated as

$$Z_j = \sum_s \left| \int_0^d [u^*_{js}(x) + v^*_{js}(x)] e^{iq_x x} \psi_0(x) dx \right|^2. \tag{5}$$

The integral of the dynamical structure factor gives the static density structure factor $S(q_x) = \int S(q_x, \omega) d\omega$, which is uniquely determined by the sum of the excitation strengths for all energy bands. Similarly, we can define the spin-density static structure factor $S_\sigma(q_x)$ and the excitation strength $Z_{\sigma j}$ by replacing $\rho^\dagger_{q_x}$ with $\sigma_z \rho^\dagger_{q_x}$. Such spin structure factors may be probed by spin-dependent Bragg spectroscopy using lasers with suitable polarization and detuning [48–50]. $S(q_x)$ and $S_\sigma(q_x)$ are related to density and spin-wave excitations, respectively. Both of them include the contributions from all of the considered energy bands.

The static structure factors for strong anisotropic spin interaction with a weak lattice $\Omega_L = 0.1E_R$ are given in Fig. 4(a) for the density and Fig. 4(b) for the spin density, where the excitation strengths Z_j and $Z_{\sigma j}$ for the first three excitation bands

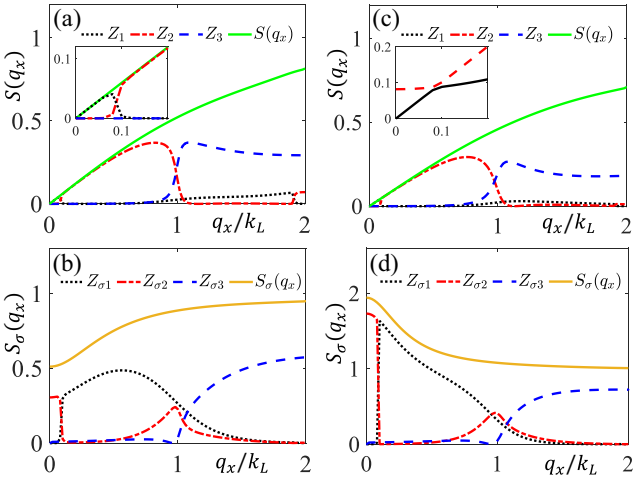

FIG. 4. Static structure factors and excitation strengths for the density in (a) and (c) and spin-density in (b) and (d). Panels (a) and (b) correspond to the excitation spectrum of the stripe phase in Fig. 2(a) and (c) and (d) correspond to the spectrum under the same parameter condition as Fig. 2(b) except $\Omega_L = 0.6E_R$. The insets in (a) and (c) show the corresponding excitation strengths and spectra near $q_x = 0$, respectively.

are also shown. $S(q_x)$ and $S_\sigma(q_x)$ increase with the quasimomentum q_x monotonically. $S(q_x)$ vanishes, but $S_\sigma(q_x)$ has a nonzero minimum value at $q_x = 0$. The excitation strengths for the first and second bands exchange at the position of the nonzero-momentum gap $q_{ac} = 0.09k_L$, showing that the first and second lowest bands correspond to density and spin excitations, respectively. This feature could be used to identify the pseudo-Goldstone modes in Bragg spectroscopy experiments.

$S(q_x)$ in the forced stripe phase for the weak anisotropic spin interaction [see Fig. 4(c)] has similar features as Fig. 4(a), while $S_\sigma(q_x)$ [see Fig. 4(d)] shows quite different properties from Fig. 4(b). In the forced stripe phase, $S_\sigma(q_x)$ decreases monotonically with q_x with a maximum at $q_x = 0$ [see Fig. 4(d)]. At the phase transition point, $S_\sigma(q_x)$ diverges as $q_x \to 0$. The dependence of $S(q_x)$ and $S_\sigma(q_x)$ on other parameters are shown in Appendix D.

In the long-wave limit, we see that the gapless Goldstone modes correspond to the density excitation (with nearly vanishing spin-density structure factor), while the gapped pseudo-Goldstone modes correspond to the spin-density excitation with finite spin-density structure factor and nearly vanishing density structure factor. Therefore, such pseudo-Goldstone modes will not be affected by additional harmonic traps in realistic experiments (which are typically spin independent and thereby only affect the density excitations), and can be observed using the spin-dependent Bragg spectroscopy.

VI. CONCLUSION

In summary, we show that the collective excitation spectrum of a spin-orbit-coupled BEC can be used to distinguish the spontaneous and forced stripe ground states induced by different symmetry breaking mechanisms. The lattice forced stripe phase, which is experimentally more accessible and robust than the spontaneous one, can provide direct experi-

mental evidence for the gapped pseudo-Goldstone spectrum. While the present work focuses on spin-orbit-coupled BECs, similar ideas can be implemented to other systems such as dipolar striped BECs [10–13], striped BECs in optical superlattice [14], or in a cavity [6–9], to study pseudo-Goldstone modes in the presence of approximate or forced symmetry breaking.

ACKNOWLEDGMENTS

We thank P. Engels, S. Mossman, E. Crowell, and T. Bersano for helpful discussions. X.-W.L., J.H., and C.Z. were supported by Air Force Office of Scientific Research (Grant No. FA9550-20-1-0220), National Science Foundation (Grant No. PHY-1806227), and Army Research Office (Grant No. W911NF-17-1-0128). G.-Q.L. acknowledges the supports from NSF of China (Grant No. 11405100), the Natural Science Basic Research Plan in Shaanxi Province of China (Grants No. 2019JM-332 and No. 2020JM-507), the Doctoral Research Fund of Shaanxi University of Science and Technology in China (Grant No. 2018BJ-02), and the China Scholarship Council (Program No. 201818610099).

APPENDIX A: METHOD

In order to calculate the excitation spectrum of the spontaneous and forced stripe phases, we first find the ground states of the system. We adopt the following ansatz:

$$(\psi_{0\uparrow}(x)\ \ \psi_{0\downarrow}(x)) = \sum_K (a_K\ \ -b_K)e^{i(K+k_0)x}, \tag{A1}$$

where $K = (2l-1)k_L$ with the integer $l = -L, ..., L+1$ represent the reciprocal lattice vectors and L is the cutoff of the plane-wave modes. The expansion coefficients a_K and b_K, together with k_0, are determined by minimizing the energy functional

$$E = \int dx\psi^\dagger(x)[H_0 + \frac{1}{2}H_{\rm int}(\psi_{0\uparrow}, \psi_{0\downarrow})]\psi(x), \tag{A2}$$

where $\psi = (\psi_{0\uparrow}, \psi_{0\downarrow})^T$ is the two-component spinor wave function normalized by the atom number $N = \int dx\psi^\dagger(x)\psi(x)$, and $H_{\rm int}(\psi_{0\uparrow}, \psi_{0\downarrow}) = {\rm diag}[gn + g_2|\psi_{0\downarrow}|^2, g_2|\psi_{0\uparrow}|^2 + gn]$ with density $n = |\psi_{0\uparrow}|^2 + |\psi_{0\downarrow}|^2$. The results for the ground state are calculated numerically by the imaginary-time evolution of the Gross-Pitaevskii (GP) equation. The corresponding initial solution is given by the variational method considering the lowest-four modes in the wave-function ansatz.

To evaluate the spectrum of elementary excitations, the Bogoliubov equation is obtained by writing the deviation of the wave function with respect to the ground state as

$$\psi_s(x,t) = e^{-i\mu t}\left[\psi_{0s}(x) + u_s(x)e^{-i\varepsilon t} + v_s^*(x)e^{i\varepsilon t}\right]. \tag{A3}$$

The perturbation amplitudes $u_s(x)$ and $v_s(x)$ with $s = \uparrow, \downarrow$ are expanded in the Bloch form in terms of the reciprocal lattice vectors:

$$u_s(x) = \sum_{m=-M}^{M+1} U_{s,m}e^{i(k_0+q_x)x+i(2m-1)k_Lx}, \tag{A4}$$

$$v_s(x) = \sum_{m=-M}^{M+1} V_{s,m}e^{i(k_0+q_x)x-i(2m-1)k_Lx}, \tag{A5}$$

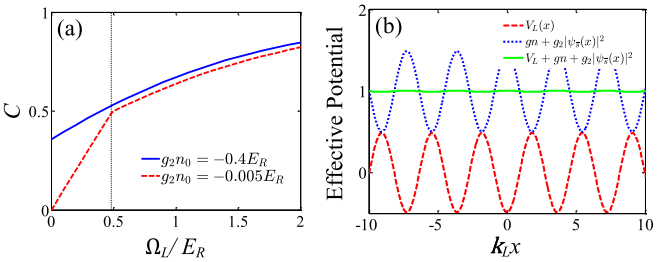

FIG. 5. (a) The modulation contrast of the ground state as a function of the strength of the optical lattice. The vertical dotted line represents the phase boundary between the plane-wave phase and the stripe phase for $g_2n_0 = -0.005E_R$. (b) The effective potential (i.e., $gn + g_2|\psi_{\bar{s}}|^2 + V_L$) of $H_{\rm GP}(\psi_{0s})$ at the phase boundary. Other parameters are $\Omega_R = 2.0E_R$, $\delta = 0$, and $gn_0 = 1.0E_R$.

where q_x is the Bloch wave vector of the excitations and M is the cutoff of the plane waves of the excited states.

APPENDIX B: GROUND STATE AND PHASE DIAGRAM

Depending on the spin-orbit coupling and the atomic interactions, the spin-orbit-coupled BEC without the optical lattice potential has three different phases: stripe, plane-wave, and zero-momentum phases [15–18,44]. The parameter range for the existence of the stripe phase is very narrow, following with the small contrast and small wavelength of the fringes, which make the observation of the stripe state very difficult in experiments. In contrast, the stripe phase in the spin-orbit-coupled BEC forced by the weak optical lattice has been observed recently [24]. The key feature is that the wavelength of the lattice beams and the Raman coupling strength are chosen such that the lattice couples two minima of the lower spin-orbit band, where the static spin-independent lattice provides a $2k_L$ momentum kick while it preserves the spin. Such a forced stripe state has a long lifetime and is more stable, and its existing parameter region is extended dramatically.

With a large Raman coupling strength like $\Omega_R = 2.0E_R$ and without the optical lattice, the stripe phase and plane wave phase appear at strong and weak anisotropic spin interaction regions, respectively. With the optical lattice, there exists a magnetized feature related with the plane-wave phase (i.e., the polarized Bloch state) in the system, which was also revealed in previous studies [51,52]. The stripe phase (i.e., unpolarized Bloch wave) for the two components exists at larger optical lattice strengths. In the formation of the stripe phase, the modulation depth of the density increases with the increasing lattice strength. The contrast of the total density $C = (n_{\rm max} - n_{\rm min})/(n_{\rm max} + n_{\rm min})$ reflects this change and shows the phase transition between the polarized Bloch state and the unpolarized Bloch state (the perfect stripe phase) for the weak anisotropic spin interaction [Fig. 5(a)].

In Fig. 1(b) of the main text, the spin polarization is plotted with respect to the optical lattice strength and the anisotropic spin interaction between atoms. For the strong anisotropic spin interaction, the existence of the stripe phase does not need the optical lattice. For the weak anisotropic spin interaction, there is a critical lattice strength Ω_L^c ($\Omega_L^c = 0.4871E_R$ for $gn_0 = 1.0E_R$ and $g_2n_0 = -0.005E_R$) for the transition from

the plane-wave phase (i.e., polarized Bloch state with $\langle\sigma_z\rangle \neq 0$) to the stripe phase (i.e., the unpolarized Bloch state with $\langle\sigma_z\rangle = 0$). We calculate the first- and second-order derivatives of the ground-state energy E with respect to the lattice strength Ω_L. The jump in the second order derivative with Ω_L shows that the phase transition is the second order. The phase transition point can also be identified from the excitation spectrum as discussed in the main text.

At the phase transition point Ω_L^c, the spatial modulation due to the atom density in the GP Hamiltonian $H_{\rm GP}(\psi_{0s})$ cancels with the spatial modulation of the lattice potential $V_L(x)$ [see Fig. 5(b)], therefore $H_{\rm GP}(\psi_{0s})$ is close to a constant at the ground state. $H_{\rm GP}(\psi_{0s})$ preserves the translational symmetry, leading to two gapless Goldstone modes shown in the inset of Fig. 2(b) in the main text. Slightly above Ω_L^c, the translational symmetry becomes approximate, leading to the pseudo-Goldstone gap. In this context, the region above Ω_L^c for the forced stripe phase resembles the spontaneous stripe phase subject to a very weak lattice perturbation (i.e., approximate symmetry region).

APPENDIX C: BOGOLIUBOV EQUATIONS

By substituting Eqs. (A3)–(A5) into Eq. (2) in the main text, the Bogoliubov equation can be obtained as follows:

$$\mathcal{H}\begin{pmatrix} u_\uparrow \\ u_\downarrow \\ v_\uparrow \\ v_\downarrow \end{pmatrix} = \varepsilon \begin{pmatrix} u_\uparrow \\ u_\downarrow \\ v_\uparrow \\ v_\downarrow \end{pmatrix}, \tag{C1}$$

where the Bogoliubov Hamiltonian

$$\mathcal{H} = \begin{pmatrix} \mathcal{H}_\uparrow & \frac{\Omega_R}{2} + g_{\uparrow\downarrow}\psi_{0\uparrow}\psi_{0\downarrow}^* & g\psi_{0\uparrow}^2 & g_{\uparrow\downarrow}\psi_{0\uparrow}\psi_{0\downarrow} \\ \frac{\Omega_R}{2} + g_{\uparrow\downarrow}\psi_{0\uparrow}^*\psi_{0\downarrow} & \mathcal{H}_\downarrow & g_{\uparrow\downarrow}\psi_{0\uparrow}\psi_{0\downarrow} & g\psi_{0\downarrow}^2 \\ -g\psi_{0\uparrow}^{*2} & -g_{\uparrow\downarrow}\psi_{0\uparrow}^*\psi_{0\downarrow}^* & -\mathcal{H}_\uparrow^* & -\frac{\Omega_R}{2} - g_{\uparrow\downarrow}\psi_{0\uparrow}^*\psi_{0\downarrow} \\ -g_{\uparrow\downarrow}\psi_{0\uparrow}^*\psi_{0\downarrow}^* & -g\psi_{0\downarrow}^{*2} & -\frac{\Omega_R}{2} - g_{\uparrow\downarrow}\psi_{0\uparrow}\psi_{0\downarrow}^* & -\mathcal{H}_\downarrow^* \end{pmatrix}, \tag{C2}$$

with

$$\mathcal{H}_\uparrow = -\partial^2/\partial x^2 + 2i\partial/\partial x - \delta/2 + V_L(x) - \mu + 2g|\psi_{0\uparrow}|^2 + g_{\uparrow\downarrow}|\psi_{0\downarrow}|^2, \tag{C3}$$

$$\mathcal{H}_\downarrow = -\partial^2/\partial x^2 - 2i\partial/\partial x + \delta/2 + V_L(x) - \mu + 2g|\psi_{0\downarrow}|^2 + g_{\uparrow\downarrow}|\psi_{0\uparrow}|^2, \tag{C4}$$

and $g_{\uparrow\downarrow} = g + g_2$. The time-independent GP equation becomes

$$\mu\psi_0 = [H_0 + H_{\rm int}(\psi_{0\uparrow}, \psi_{0\downarrow})]\psi_0. \tag{C5}$$

The ground state ψ_0 and the chemical potential μ are obtained by the imaginary-time evolution. The Bogoliubov excitation energy ε with respect to q_x is numerically obtained by diagonalizing the Bogoliubov Hamiltonian.

Besides the Raman detuning δ demonstrated in Figs. 2(c), 2(d) and 3 in the main text, the effects of other tunable parameters (Raman coupling and atomic interactions) on the elementary excitations are shown in Fig. 6. The effect of the Raman coupling on zero-momentum gap Δ_{ε_0} is shown in Fig. 6(a), where the critical lattice strength for the minimum of the zero-momentum gap increases with the increasing Raman coupling strength. The effect of the atomic interactions on Δ_{ε_0} is shown in Fig. 6(b), where the curves are shifted to larger optical lattice strength when the atomic interaction gn_0 increases.

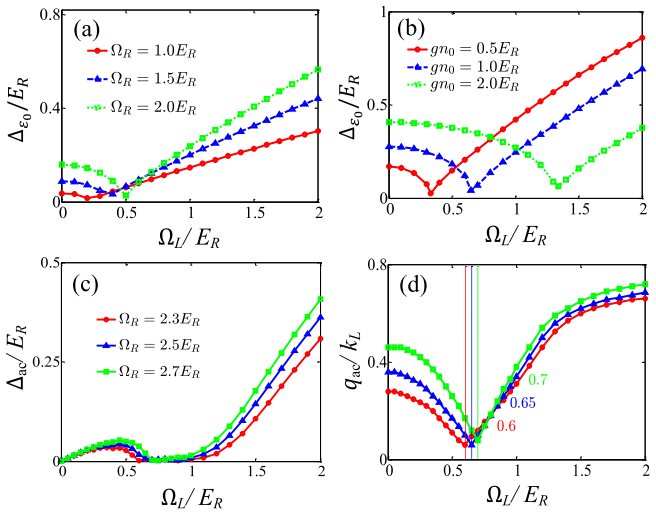

FIG. 6. (a),(b) The zero-momentum gap Δ_{ε_0} as a function of lattice strength Ω_L for different Ω_R (a) and gn_0 (b). (c),(d) $\Delta_{\rm ac}$ (c) and $q_{\rm ac}$ (d) of the avoided crossing gap as functions of Ω_L for $\Omega_R = 2.3E_R$ (dots), $\Omega_R = 2.5E_R$ (triangles), and $\Omega_R = 2.7E_R$ (squares); $q_{\rm ac}$ reaches its minimum at $\Omega_L = 0.6E_R$, $0.65E_R$, and $0.7E_R$, respectively. The other parameters are $\delta = 0$, $gn_0 = 1.0E_R$ and $g_2 = -0.005E_R$.

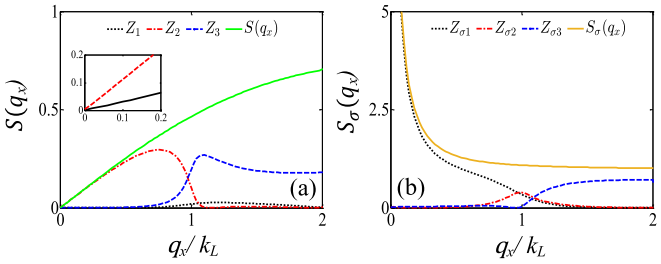

FIG. 7. Static structure factors and excitation strengths for density (a) and spin density (b) at the critical lattice strength $\Omega_L^c = 0.4871E_R$. The inset in (a) corresponds to two lowest energy bands in the small momentum region. Other parameters are $\Omega_R = 2.0E_R$, $gn_0 = 1.0E_R$, and $g_2 n_0 = -0.005E_R$.

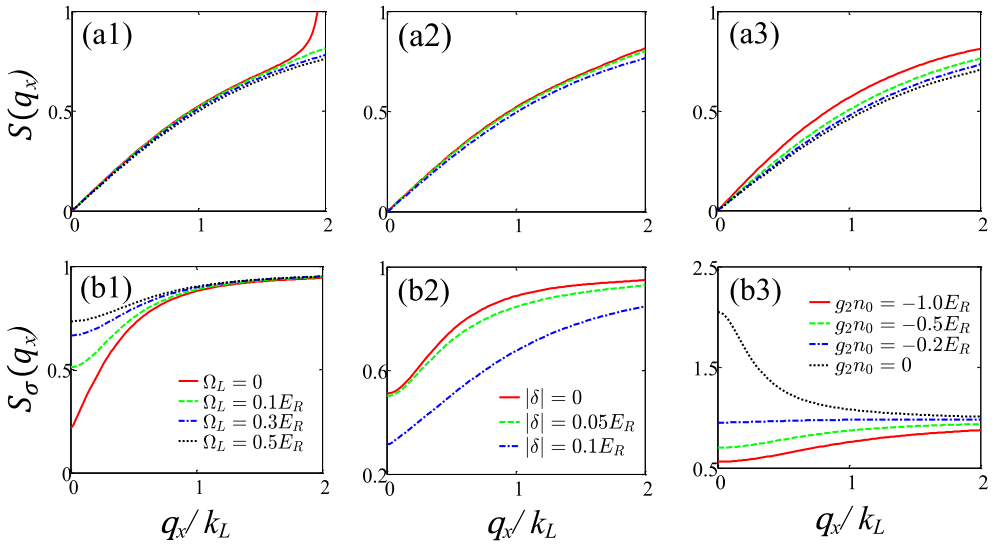

FIG. 8. Change of the static structure factors for density (a1)–(a3) and spin-density (b1)–(b3) with different parameters Ω_L, δ, and g_2n_0. (a1),(b1) $\delta = 0$, $\Omega_R = 2.0E_R$, $gn_0 = 1.0E_R$, and $g_2n_0 = -0.4E_R$; (a2),(b2) $\Omega_R = 2.0E_R$, $\Omega_L = 0.1E_R$, $gn_0 = 1.0E_R$, and $g_2n_0 = -0.4E_R$; (a3),(b3) $\delta = 0$, $\Omega_R = 2.0E_R$, $\Omega_L = 0.6E_R$, and $gn_0 = 1.0E_R$.

The effects of the Raman coupling on the size and position of nonzero-momentum gap Δ_{ac} are shown in Figs. 6(c) and 6(d). The size of Δ_{ac} increases with the increasing Raman coupling strength except at some crossing points. The minimum position of the nonzero-momentum gap shifts to the larger optical lattice strength for larger Raman coupling strength.

APPENDIX D: DYNAMICAL STRUCTURE FACTOR AND BRAGG SPECTROSCOPY MEASUREMENT

The Bragg spectroscopy measures the dynamical structure factor of the BEC, i.e., the density response of the system to the external perturbation generated by the scattering probe of momentum $\hbar q_x$, and energy $\hbar\omega$ [44,47]. Denoting the linear perturbation $V_1 = \frac{V}{2}[\rho^\dagger_{q_x} e^{-i\omega t} + \rho_{-q_x} e^{i\omega t}]$, where $\rho_{q_x} = \sum_j e^{iq_x x_j/\hbar}$ is the Fourier transformation of one-body density operator with the probe momenta q_x, the dynamical structure factor takes the form

$$S(q_x, \omega) = \sum_j |\langle j|\rho^\dagger_{q_x}|0\rangle|^2 \tilde{\delta}[\hbar\omega - (E_j - E_0)]. \quad \text{(D1)}$$

Here, $|0\rangle$ ($|j\rangle$) is the ground (excited) state with the energy E_0 (E_j). We can define the spin structure factor S_σ in a similar way, which can be measured using spin-dependent Bragg spectroscopy [48–50].

The static structure factors and excitation strengths for the density and spin density are given in Figs. 7(a) and 7(b) for the phase transition point $\Omega_L^c = 0.4871E_R$. At Ω_L^c, the excitation spectrum contains two gapless Goldstone modes although the anisotropic spin interaction is weak. $S(q_x)$ has a very similar feature as the spontaneous stripe phase, while $S_\sigma(q_x)$ shows a divergence at $q_x \to 0$. The effects of other external parameters on $S(q_x)$ and $S_\sigma(q_x)$ are given in Fig. 8. As shown in Figs. 8(a1)–8(a3), $S(q_x = 0) = 0$, independent of parameters. The dependence of $S(q_x)$ on other parameters is generally very weak.

In contrast, $S_\sigma(q_x)$ shows strong dependence on other parameters. It increases with increasing optical lattice strength Ω_L [Fig. 8(b1)], but decreases with increasing Raman detuning $|\delta|$ [Fig. 8(b2)]. $S_\sigma(q_x)$ is larger for weaker anisotropic spin interaction [Fig. 8(b3)]. Interestingly, Fig. 8(b3) shows that $S_\sigma(q_x)$ increases (decreases) monotonically with the momentum for strong (weak) anisotropic spin interaction, therefore has maximum (minimum) at $q_x = 0$. This result was also shown in Fig. 4 in the main text.

[1] M. Boninsegni and N. V. Prokofv, Colloquium: Supersolids: What and where are they?, Rev. Mod. Phys. **84**, 759 (2012).

[2] D. J. Thouless, The flow of a dense superfluid, Ann. Phys. **52**, 403 (1969).

[3] A. F. Andreev and I. M. Lifshitz, Quantum theory of defects in crystals, Sov. Phys. JETP **29**, 1107 (1969).

[4] E. Kim and M. H. W. Chan, Probable observation of a supersolid helium phase, Nature (London) **427**, 225 (2004).

[5] D. Y. Kim and M. H. W. Chan, Absence of Supersolidity in Solid Helium in Porous Vycor Glass, Phys. Rev. Lett. **109**, 155301 (2012).

[6] F. Cinti, T. Macrí, W. Lechner, G. Pupillo, and T. Pohl, Defect-induced supersolidity with soft-core bosons, Nat. Commun. **5**, 3235 (2014).

[7] K. Baumann, C. Guerlin, F. Brennecke, and T. Esslinger, Dicke quantum phase transition with a superfluid gas in an optical cavity, Nature (London) **464**, 1301 (2010).

[8] H. Keß ler, J. Klinder, M. Wolke, and A. Hemmerich, Steering Matter Wave Superradiance with an Ultranarrow-Band Optical Cavity, Phys. Rev. Lett. **113**, 070404 (2014).

[9] J. Léonard, A. Morales, P. Zupancic, T. Esslinger, and T. Donner, Supersolid formation in a quantum gas breaking a

continuous translational symmetry, Nature (London) **543**, 87 (2017).

[10] L. Tanzi, E. Lucioni, F. Famá, J. Catani, A. Fioretti, C. Gabbanini, R. N. Bisset, L. Santos, and G. Modugno, Observation of a Dipolar Quantum Gas with Metastable Supersolid Properties, Phys. Rev. Lett. **122**, 130405 (2019).

[11] F. Böttcher, J.-N. Schmidt, M. Wenzel, J. Hertkorn, M. Guo, T. Langen, and T. Pfau, Transient Supersolid Properties in an Array of Dipolar Quantum Droplets, Phys. Rev. X **9**, 011051 (2019).

[12] L. Chomaz, D. Petter, P. Ilzhöfer, G. Natale, A. Trautmann, C. Politi, G. Durastante, R. M. W. van Bijnen, A. Patscheider, M. Sohmen, M. J. Mark, and F. Ferlaino, Long-Lived and Transient Supersolid Behaviors in Dipolar Quantum Gases, Phys. Rev. X **9**, 021012 (2019).

[13] G. Natale, R. M. W. van Bijnen, A. Patscheider, D. Petter, M. J. Mark, L. Chomaz, and F. Ferlaino, Excitation Spectrum of a Trapped Dipolar Supersolid and Its Experimental Evidence, Phys. Rev. Lett. **123**, 050402 (2019).

[14] J.-R. Li, J. Lee, W. Huang, S. Burchesky, B. Shteynas, F. C. Top, A. O. Jamison, and W. Ketterle, A stripe phase with supersolid properties in spin-orbit-coupled Bose-Einstein condensates, Nature (London) **543**, 91 (2017).

[15] C. J. Wang, C. Gao, C.-M. Jian, and H. Zhai, Spin-Orbit Coupled Spinor Bose-Einstein Condensates, Phys. Rev. Lett. **105**, 160403 (2010).

[16] T.-L. Ho and S. Zhang, Bose-Einstein Condensates with Spin-Orbit Interaction, Phys. Rev. Lett. **107**, 150403 (2011).

[17] Y.-J. Lin, K. Jiménez-García, and I. B. Spielman, Spin-orbit-coupled Bose-Einstein condensates, Nature (London) **471**, 83 (2011).

[18] Y. Li, L. P. Pitaevskii, and S. Stringari, Quantum Tricriticality and Phase Transitions in Spin-Orbit Coupled Bose-Einstein Condensates, Phys. Rev. Lett. **108**, 225301 (2012).

[19] C. Wu, I. M. Shem, and X.-F. Zhou, Unconventional Bose-Einstein condensations from spin-orbit coupling, Chin. Phys. Lett. **28**, 097102 (2011).

[20] H. Hu, B. Ramachandhran, H. Pu, and X.-J. Liu, Spin-Orbit Coupled Weakly Interacting Bose-Einstein Condensates in Harmonic Traps, Phys. Rev. Lett. **108**, 010402 (2012).

[21] Y. Zhang, L. Mao, and C. Zhang, Mean-Field Dynamics of Spin-Orbit Coupled Bose-Einstein Condensates, Phys. Rev. Lett. **108**, 035302 (2012).

[22] J. Sánchez-Baena, J. Boronat, and F. Mazzanti, Supersolid stripes enhanced by correlations in a Raman spin-orbit-coupled system, Phys. Rev. A **101**, 043602 (2020).

[23] X.-W. Luo, K. Sun, and C. Zhang, Spin-Tensor-Momentum-Coupled Bose-Einstein Condensates, Phys. Rev. Lett. **119**, 193001 (2017).

[24] T. M. Bersano, J. Hou, S. Mossman, V. Gokhroo, X.-W. Luo, K. Sun, C. Zhang, and P. Engels, Experimental realization of a long-lived striped Bose-Einstein condensate induced by momentum-space hopping, Phys. Rev. A **99**, 051602(R) (2019).

[25] J. Goldstone, A. Salam, and S. Weinberg, Broken symmetries, Phys. Rev. **127**, 965 (1962).

[26] C. P. Burgess, Goldstone and pseudo-Goldstone bosons in nuclear, particle and condensed-matter physics, Phys. Rep. **330**, 193 (2000).

[27] S. Weinberg, Approximate Symmetries and Pseudo-Goldstone Bosons, Phys. Rev. Lett. **29**, 1698 (1972).

[28] Y. Nambu, Axial vector current conservation in weak interactions, Rev. Mod. Lett. **4**, 380 (1960).

[29] Y. Nambu and G. Jona-Lasinio, Dynamical model of elementary particles based on an analogy with superconductivity. I, Phys. Rev. **122**, 345 (1961).

[30] M. Tanabashi *et al.*, Review of particle physics, Phys. Rev. D **98**, 030001 (2018).

[31] Y. Nambu, Quasi-Particles and gauge invariance in the theory of superconductivity, Phys. Rev. **117**, 648 (1960).

[32] M. Hartmann, F. Mielke, J. P. Toennies, A. F. Vilesov, and G. Benedek, Direct Spectroscopic Observation of Elementary Excitations in Superfluid He Droplets, Phys. Rev. Lett. **76**, 4560 (1996).

[33] E. Demler, W. Hanke, and S.-C. Zhang, SO(5) theory of antiferromagnetism and superconductivity, Rev. Mod. Phys. **76**, 909 (2004).

[34] R. M. Fernandes and A. V. Chubukov, Low-energy microscopic models for iron-based superconductors: A review, Rep. Prog. Phys. **80**, 014503 (2017).

[35] A. V. Chumak, V. I. Vasyuchka, A. A. Serga, and B. Hillebrands, Magnon spintronics, Nat. Phys. **11**, 453 (2015).

[36] C. L. Henley, Ordering Due to Disorder in a Frustrated Vector Antiferromagnet, Phys. Rev. Lett. **62**, 2056 (1989).

[37] J. G. Rau, P. A. McClarty, and R. Moessner, Pseudo-Goldstone Gaps and Order-by-Quantum Disorder in Frustrated Magnets, Phys. Rev. Lett. **121**, 237201 (2018).

[38] J. Stenger, S. Inouye, A. P. Chikkatur, D. M. Stamper-Kurn, D. E. Pritchard, and W. Ketterle, Bragg Spectroscopy of a Bose-Einstein Condensate, Phys. Rev. Lett. **82**, 4569 (1999).

[39] J. Steinhauer, R. Ozeri, N. Katz, and N. Davidson, Excitation Spectrum of a Bose-Einstein Condensate, Phys. Rev. Lett. **88**, 120407 (2002).

[40] M. A. Khamehchi, Y. Zhang, C. Hamner, T. Busch, and P. Engels, Measurement of collective excitations in a spin-orbit-coupled Bose-Einstein condensate, Phys. Rev. A **90**, 063624 (2014).

[41] S.-C. Ji, L. Zhang, X.-T. Xu, Z. Wu, Y. Deng, S. Chen, and J.-W. Pan, Softening of Roton and Phonon Modes in a Bose-Einstein Condensate with Spin-Orbit Coupling, Phys. Rev. Lett. **114**, 105301 (2015).

[42] R. Mottl, F. Brennecke, K. Baumann, R. Landig, T. Donner, T. Esslinger, Roton-Type mode softening in a quantum gas with cavity-mediated long-range interactions, Science **336**, 1570 (2012).

[43] L.-C. Ha, L. W. Clark, C. V. Parker, B. M. Anderson, and C. Chin, Roton-Maxon Excitation Spectrum of Bose Condensates in a Shaken Optical Lattice, Phys. Rev. Lett. **114**, 055301 (2015).

[44] Y. Li, G. I. Martone, L. P. Pitaevskii, and S. Stringari, Superstripes and the Excitation Spectrum of a Spin-Orbit-Coupled Bose-Einstein Condensate, Phys. Rev. Lett. **110**, 235302 (2013).

[45] X.-L. Chen, J. Wang, Y. Li, X.-J. Liu, and H. Hu, Quantum depletion and superfluid density of a supersolid in Raman spin-orbit-coupled Bose gases, Phys. Rev. A **98**, 013614 (2018).

[46] L. Chen, H. Pu, Z.-Q. Yu, and Y. Zhang, Collective excitation of a trapped Bose-Einstein condensate with spin-orbit coupling, Phys. Rev. A **95**, 033616 (2017).

[47] L. Pitaevskii and S. Stringari, *Bose-Einstein Condensation and Superfluidity* (Oxford University Press, Oxford, 2016).

[48] D. Baillie and P. B. Blakie, Spin-dependent Bragg spectroscopy of a spinor Bose gas, Phys. Rev. A **93**, 033607 (2016).

[49] S. Hoinka, M. Lingham, M. Delehaye, and C. J. Vale, Dynamic Spin Response of a Strongly Interacting Fermi Gas, Phys. Rev. Lett. **109**, 050403 (2012).

[50] I. Carusotto, Bragg scattering and the spin structure factor of two-component atomic gases, J. Phys. B **39**, S211 (2006).

[51] G. I. Martone, T. Ozawa, C. Qu, and S. Stringari, Optical-lattice-assisted magnetic phase transition in a spin-orbit-coupled Bose-Einstein condensate, Phys. Rev. A **94**, 043629 (2016).

[52] Z. Chen and Z. Liang, Ground-state phase diagram of a spin-orbit-coupled bosonic superfluid in an optical lattice, Phys. Rev. A **93**, 013601 (2016).